Engineering Entropy-Driven Reactions and Networks Catalyzed by DNA

David Yu Zhang, *et al.*

Science **318**, 1121 (2007);
DOI: 10.1126/science.1148532

oped a new quantum analysis (i.e., SRS initiation from spontaneous emission) generalized to an arbitrary number of Stokes and anti-Stokes (S/AS) lines to investigate the mutual coherence of these sidebands (*15*). The results, applied to an isolated vibrational (or rotational) Raman transition, predict that in the high-gain transient regime, all S/AS sidebands carry phases that are automatically correlated in a deterministic manner (i.e., phase-locked). Indeed, even though the spontaneous seed for the S1 pulse is temporally and spatially randomly fluctuating during the generation process, this noise is heavily filtered out under the high-gain transient conditions to leave out a Stokes field with a single overall phase. Concomitantly with the generation of S1, there is a rise of a first anti-Stokes (AS1) field and a molecular excitation, which are determined by the same phase that arises spontaneously (*22, 23*). This result is ascertained by calculating the degree of mutual coherence between the Stokes and anti-Stokes fields (*15*).

More importantly, the theory shows that both the higher-order S/AS pairs and the molecular excitation retain the same key features of sharing a common phase related to that of the first S/AS pair. The observed high efficiency of the Raman conversion indicates that we were able to excite substantial molecular coherence even though it was initiated from quantum noise. In analogy with the adiabatic regime (*4*), the results of the new theory can be viewed as the generation of a coherent molecular spatial excitation, which modulates the first S/AS pair by adding S/AS sidebands. These then become modulated to generate sidebands of their own, and so on.

The spectrum generated with circular polarization contains both rotation- and vibration-generated lines. Consequently, there is a second coherent molecular excitation, implying the introduction of one additional random phase. This in itself does not destroy the phase coherence of either the pure vibrational or the pure rotational spectra, but to experimentally produce sub-fs pulses, these degrees of freedom need to be relatively controlled to correct for this additional random phase. Also, one could optimize the medium pressure to suppress completely the vibrational lines (*6*), leaving only the mutually coherent rotational lines.

The extension of using this HC-PCF in other Raman excitation regimes is straightforward. For example, its combination with the adiabatic preparation technique would enhance the conversion efficiency and further reduce the required pumping powers involved while ensuring better control over the spectral components' phases. This would enable the generation and synthesis of attosecond pulses with much lower pumping powers. Furthermore, in addition to the intrinsic fundamental importance of the discovery of this "Von Neumann–Wigner"–related waveguidance to photonics, it will provide us with new tools to develop next-generation HC-PCFs with even broader bandwidth and lower transmission loss. For example, with lower loss figures, one could synthesize ultrashort pulses using continuous-wave pumps. This would permit the synthesis of arbitrary optical waveforms with a degree of control approaching that in electronics.

References and Notes

1. P. B. Corkum, *Phys. Rev. Lett.* **71**, 1994 (1993).
2. S. Baker *et al.*, *Science* **312**, 424 (2006).
3. M. Uiberacker *et al.*, *Nature* **446**, 627 (2007).
4. A. V. Sokolov, D. R. Walker, D. D. Yavuz, G. Y. Yin, S. E. Harris, *Phys. Rev. Lett.* **85**, 562 (2000).
5. A. Nazarkin, G. Korn, M. Wittmann, T. Elsaesser, *Phys. Rev. Lett.* 83, 2560 LP (1999).
6. H. Kawano, Y. Hirakawa, T. Imasaka, *IEEE J. Quantum Electron.* 34, 260 (1998).
7. E. Sali, K. J. Mendham, J. W. G. Tisch, T. Halfmann, J. P. Marangos, *Opt. Lett.* **29**, 495 (2004).
8. F. Benabid, J. C. Knight, G. Antonopoulos, P. S. J. Russell, *Science* **298**, 399 (2002).
9. F. Benabid, *Philos. Trans. R. Soc. London A* **364**, 3439 (2006).
10. F. Benabid, G. Bouwmans, J. C. Knight, P. S. J. Russell, F. Couny, *Phys. Rev. Lett.* **93**, 123903 (2004).
11. F. Benabid, F. Couny, J. C. Knight, T. A. Birks, P. S. J. Russell, *Nature* **434**, 488 (2005).
12. P. J. Roberts *et al.*, *Opt. Express* **13**, 236 (2005).
13. J. v. Neumann, E. Wigner, *Phys. Z.* **30**, 465 (1929).
14. F. H. Stillinger, D. R. Herrick, *Phys. Rev. A* **11**, 446 (1975).
15. Supporting online material is available on *Science* Online.
16. F. Couny, F. Benabid, P. S. Light, *Opt. Lett.* **31**, 3574 (2006).
17. G. Humbert *et al.*, *Opt. Express* **12**, 1477 (2004).
18. A. Argyros, J. Pla, *Opt. Express* **15**, 7713 (2007).
19. S. E. Harris, A. V. Sokolov, *Phys. Rev. Lett.* **81**, 2894 (1998).
20. H. Kawano, Y. Hirakawa, T. Imasaka, *Appl. Phys. B* **65**, 1 (1997).
21. F. Benabid, G. Antonopoulos, J. C. Knight, P. S. J. Russell, *Phys. Rev. Lett.* **95**, 213903 (2005).
22. W. Wasilewski, M. G. Raymer, *Phys. Rev. A* **73**, 063816 (2006).
23. S. Y. Kilin, *Europhys. Lett.* **5**, 419 (1988).
24. We are grateful to T. Birks, D. Bird, and C. Wu for stimulating discussions. This work is funded by the UK Engineering and Physical Sciences Research Council (EPSRC). M.G.R. was supported by the U.S. NSF (grants ECS-0621723/PHYS-0456974/PHYS-0554842).

Engineering Entropy-Driven Reactions and Networks Catalyzed by DNA

David Yu Zhang,[1]† Andrew J. Turberfield,[2] Bernard Yurke,[3]* Erik Winfree[1]†

Artificial biochemical circuits are likely to play as large a role in biological engineering as electrical circuits have played in the engineering of electromechanical devices. Toward that end, nucleic acids provide a designable substrate for the regulation of biochemical reactions. However, it has been difficult to incorporate signal amplification components. We introduce a design strategy that allows a specified input oligonucleotide to catalyze the release of a specified output oligonucleotide, which in turn can serve as a catalyst for other reactions. This reaction, which is driven forward by the configurational entropy of the released molecule, provides an amplifying circuit element that is simple, fast, modular, composable, and robust. We have constructed and characterized several circuits that amplify nucleic acid signals, including a feedforward cascade with quadratic kinetics and a positive feedback circuit with exponential growth kinetics.

The development of modular biochemical circuit elements poses several challenges. First, distinct signals must be carried by distinct chemical species, motivating the use of information-carrying molecules whose sequences can be used to encode signal identity. Second, "wiring up" a gate to specified inputs and outputs involves the design and synthesis of new molecules; this calls for modular gate designs. Third, a fast and robust catalytic mechanism must be identified and coupled to a suitable energy source in order to create gates with signal gain. Fourth, it must be possible to construct circuits of arbitrary complexity that can produce an unlimited variety of dynamical behaviors. Finally, there should be no leak or crosstalk between distinct signals and gates. It is difficult to meet all these challenges simultaneously.

Nucleic acids are attractive for this purpose because the combinatorial sequence space allows for an enormous diversity of signal carriers, and the predictability and specificity of Watson-Crick base pairing facilitate the design of gate architectures. The "RNA world" hypothesis further suggests that sophisticated biochemical organization can be achieved with nucleic acids alone (*1*), and nucleic acids have indeed been shown to be a versatile construction material for engineering molecular structures and devices (*2, 3*), including catalytic (*4–8*) and logical (*9–12*) control elements and circuits (*13–17*). Engineering (deoxy)ribozyme-based logic gates has been very effective, resulting in systems containing over 100 gates operating independently in parallel (*10*) as well as systems demonstrating cascading of a signal between two gates (*13, 15, 16*). Alternatively, hybridization-based systems, usually driven by the energy of base-pair formation, have proven especially suitable for cascading signals, as demonstrated by a circuit five layers deep (*17*). That work, relying primarily on noncatalytic logic gates, identified amplification and signal gain as essential for scaling up to large cascaded circuits. We provide a solution to this problem.

1121

The entropy-driven catalytic gate presented here is substantially simpler than previous hybridization-based designs; moreover, it is faster, better understood, and more modular. The net reaction is shown in Fig. 1A: Fuel strand (F) reacts with the three-stranded substrate complex (S), displacing output and signal strands (OB and SB) from linker strand (LB) to form waste complex (W). The total number of base pairs in the reactants and products is unchanged; the reaction is driven forward thermodynamically by the entropic gain of the liberated molecules. Fuel, signal, catalyst, and output are all single-stranded DNA molecules that can be of similar lengths; thus, each molecule may play multiple roles within a network. For example, the output of one gate may serve as the input to another. Notably, catalyst C and output OB may be entirely independent in sequence (18); this modularity implies that a catalytic gate can be designed to act at any point within a preexisting circuit. Unlike previous hybridization-based catalyst systems, the reaction design does not require unusual secondary structures such as pseudoknots and kissing loops. Undesired interactions can be avoided by design (19–21), resulting in reliable and predictable circuit behavior.
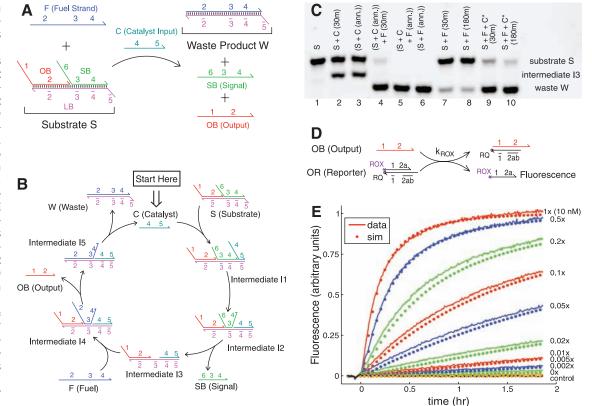
Strands are conceptually subdivided into functional domains (number labels in Fig. 1) whose sequences determine the pattern of interactions between circuit components. [Domain sequences are given in Table 1; see supporting online material (SOM) text S1 for design details.] The domains can be grouped by purpose: domains 3 and 5 are termed toehold domains, whereas domains 1, 2, 4, and 6 are termed specificity domains. Toehold domains are short enough to bind only fleetingly in the absence of additional binding (and need not be distinct), but they greatly accelerate the initiation of strand displacement reactions (22). Specificity domains ensure specific interactions [even a single mismatch can slow down branch migration substantially (23)] and determine the identities of the catalyst and output molecules. The lengths of the toehold domains determine kinetics and need to be between roughly 4 and 10 nucleotides (nt), but the specificity domains may be of any length sufficient to ensure thermal stability. Domains 1 and 6 of OB and SB, respectively, are inert, whereas their respective toeholds are sequestered in S.

Catalytic activity has two characteristic behaviors: the speedup of the target reaction and the re-release of the catalyst to allow for multiple turnover. To achieve these behaviors, we introduce and apply a design principle that we call toehold exchange (Fig. 1B): C first binds to the single-stranded toehold domain $\overline{5}$ on S to form the four-stranded intermediate I1, which then rearranges (by branch migration) to form I2. The binding between toehold domains 3 and $\overline{3}$ is too weak to keep SB attached, so I2 spontaneously dissociates into SB and I3. Newly exposed $\overline{3}$ then facilitates the binding of F, resulting in I4, which then quickly rearranges to release OB and I5. Finally, I5 rearranges so that C is attached only by the binding of 5 and $\overline{5}$, which spontaneously dissociates to leave W and regenerate C. The reaction mechanism presented here, based on branch migration and driven by entropy, differs from the traditional view of catalysis in biological organisms in that it requires no enzymes and alters no covalent bonds.

It is important to ensure that alternative interactions do not interfere with intended gate functions. Toward this end, a key design principle is that the complements of the specificity domains never appear in their single-stranded

[1]Computation and Neural Systems, California Institute of Technology, MC 136-93, 1200 East California Boulevard, Pasadena, CA 91125, USA. [2]Department of Physics, University of Oxford, Clarendon Laboratory, Parks Road, Oxford OX1 3PU, UK. [3]Bell Laboratories, Alcatel-Lucent, Murray Hill, NJ 07974, USA.

*Present address: Materials Science and Engineering Department, Boise State University, Boise, ID 83725, USA.
†To whom correspondence should be addressed. E-mail: winfree@caltech.edu (E.W.); dzhang@dna.caltech.edu (D.Y.Z.)

Fig. 1. The entropy-driven reaction. (**A**) System components. Number labels denote functional domains, which are continuous stretches of DNA that act as units in binding. Domain $\overline{x}$ is the complement of (and will hybridize to) domain x. (**B**) The proposed catalytic pathway. Reverse reactions are also present and modeled (with the exception of $I5+OB \rightarrow I4$, which occurs at a negligible rate). (**C**) Analysis by PAGE (12% native gel) of the reaction mechanism. Unless otherwise noted, all experiments were performed at 25°C in tris-acetate (TE) buffer supplemented with 12.5 mM MgCl$_2$. Here, $[S] = [F] = 200$ nM. $[C] = 200$ nM, except where C^* denotes 20 nM. "ann." denotes that species were annealed; "30 m" denotes that the reaction occurred for 30 min. See fig. S5 for the full gel, including control lanes. (**D**) Fluorescent reporter strategy. ROX denotes the carboxy-X-rhodamine fluorophore, and RQ denotes the Iowa Black Red Quencher. Domain 2 is subdivided into 2a, 2b, and 2c; 2ab consists of 2a and 2b (Table 1). (**E**) Demonstration of catalysis. Different amounts of C were introduced into the system at $t \approx 0$. Here, $[S] = 10$ nM = 1×, $[F] = 13$ nM, and $[OR] = 30$ nM.

Fluorescence (in all figures) is reported in units such that 0.0 is the background fluorescence of the quenched reporter and 1.0 is the fluorescence of ~10 nM of triggered reporter. The control trace (black) shows the reaction with no substrate S and no catalyst C. Dotted lines show curves calculated with the reduced reaction model. sim, simulated.

form. Except at toeholds, no two molecules interact with each other via complementary single-stranded domains. The catalytic gate is therefore expected to function for most choices of domain sequences lacking strong secondary structure and spurious mutual interactions (*19–21*).

In Fig. 1C, polyacrylamide gel electrophoresis (PAGE) is used to verify the catalytic pathway (*24*). By reacting substrate *S* (purified by gel) and catalyst *C* in the absence of fuel *F*, we prevent the reaction from progressing past intermediate *I3*. The amount of *I3* produced after 30 min (lane 2) is almost identical to that present at equilibrium, as assessed by annealing
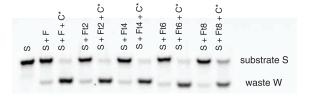
the reaction components (lane 3). This suggests that all reactions up to *I3* are fast on this time scale. Similarly, the subsequent reaction between *I3* and *F* is also fast (lanes 3 to 5). The complete system behaves as expected: The uncatalyzed reaction is slow (lanes 7 and 8), and a substoichiometric quantity (0.1×) of *C* enables the reaction to proceed rapidly to near-completion (lanes 9 and 10).

In order to measure the time course of the catalyzed reaction by means of a fluorescent reporter without interference from fluorophore-quencher interactions (*25*) (SOM text S3), we use an indirect reporter complex *OR*. *OR* reacts

stochiometrically with output *OB* to separate a fluorophore-labeled strand from a quencher-labeled strand, thereby increasing fluorescence (Fig. 1D). The rate constant for the reporter system was measured to be $k_{\mathrm{ROX}} = 4 \cdot 10^5 \mathrm{M}^{-1}\mathrm{s}^{-1}$ (SOM text S4). Because initial [*OR*] = 30 nM is in excess to [*S*] = 10 nM, the reporter complex remains substantially in excess, and the reporting delay should remain less than 100 s, which is short as compared to the half time of the catalyzed reactions. *OR* does not react substantially with *S*, because there are no single-stranded toeholds to initiate interaction. Measurements of the kinetics of the catalyzed reaction over a 500-fold range of catalyst concentration are shown in Fig. 1E.

We modeled this system using the reduced reaction set shown below.

$$S + F \xrightarrow{k_0} SB + OB + W$$
$$S + C \underset{k_{-1}}{\overset{k_1}{\rightleftharpoons}} I3 + SB$$
$$I3 + F \xrightarrow{k_2} I5 + OB$$
$$I5 \underset{k_{-3}}{\overset{k_3}{\rightleftharpoons}} C + W$$
$$OB + OR \xrightarrow{k_{\mathrm{ROX}}} \text{Fluorescence}$$

where $k_0 = 2.3 \cdot 10^1 \mathrm{M}^{-1}\mathrm{s}^{-1}$,
$$k_1 = 6.5 \cdot 10^5 \mathrm{M}^{-1}\mathrm{s}^{-1},$$
$$k_2 = 4.2 \cdot 10^5 \mathrm{M}^{-1}\mathrm{s}^{-1},$$
$$k_3 = 4 \cdot 10^{-3}\mathrm{s}^{-1} (\text{fitted}), \text{and}$$
$$k_{\mathrm{ROX}} = 4 \cdot 10^5 \mathrm{M}^{-1}\mathrm{s}^{-1}$$

The first reaction shown models the uncatalyzed (leak) reaction. Intermediate steps in branch-migration reactions are omitted, because they are relatively fast at experimental concentrations (SOM text S5) (*26*) and because intermediates *I1*, *I2*, and *I4* are not observed in PAGE analysis of reactants and products (Fig. 1C). Noting the approximate symmetry between the corresponding reactions, we assume that $k_{-3} = k_1$ and $k_{-1} = k_2$. The rate constants k_0, k_1, and k_2 were measured individually (fig. S4); k_3 was fit to the data of Fig. 1E. The time course of the catalyzed reaction over a wide range of catalyst concentrations is accurately reproduced by this reduced system of rate equations (Fig. 1E). According to this model, the addition of catalyst can accelerate the reaction by over four orders of magnitude ($k_2/k_0 = 1.8 \cdot 10^4$).

In the net reaction, each base pair that is broken is replaced by another of the same type, so the net free energy change from base-pairing interactions should be small. The reaction is driven by the gain in configurational entropy corresponding to the liberation of *OB* and *SB* at the cost of localizing *F*. To confirm the dominance of this entropic driving force, we truncate *F* by removing up to 8 nt from its 5′ end, making the products more and more thermodynamically disfavored. Nonetheless, in all cases

Table 1. Domain sequences of basic catalytic reaction.

Domain	Sequence	Length (nt)
1	5′-CTTTCCTACA-3′	10
2a	5′-CCTACG-3′	6
2b	5′-TCTCCA-3′	6
2c	5′-ACTAACTTACGG-3′	12
3	5′-CCCT-3′	4
4	5′-CATTCAATACCCTACG-3′	16
5	5′-TCTCCA-3′	6
6	5′-CCACATACATCATATT-3′	16

Fig. 2. Verification of entropic driving force. Analysis by PAGE (12% native gel) of reactions with truncated fuel strands. [*S*] = [*F*] = 200 nM. [*C*] = 20 nM, as denoted by the asterisk. All reactions were run at 25°C for 3 hours. "Ft2" denotes that two bases were truncated from the 5′ end of fuel strand *F*.
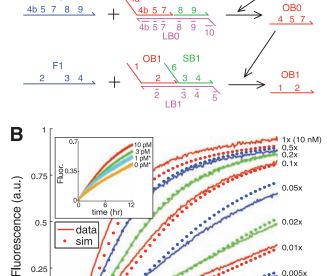

Fig. 3. A two-layer cascaded network. (**A**) Schematic. See table S2 for sequences of new domains. (**B**) Kinetics. Indicated amounts of initial catalyst *C0* were added at $t \approx 0$. Fluorescence derives from reporter complex *OR* (Fig. 1D) at 30 nM. Dotted lines show simulated traces; see SOM text S8 for details on reaction rates and modeling. a.u., arbitrary units. (Inset) Response to 0.0010×, 0.0003×, and 0.0001× catalyst. The asterisk indicates that three independent reaction traces are shown. 1.0 fluorescence units correspond to ≈ 10 nM of triggered reporter.

the waste product is favored at equilibrium (Fig. 2; see SOM text S6 for discussion on entropy and free energies). The thermodynamic driving force, being dominated by center-of-mass configurational entropy of released molecules, is somewhat robust to environmental conditions such as temperature and salt concentrations that alter the strength of DNA hybridization (SOM text S7 and fig. S6).

To demonstrate cascaded circuit construction, we designed a two-layer feedforward network by introducing an upstream catalyst system whose output acts as the catalyst for the original system (Fig. 3A). For clarity, F, OB, and the other reactants and products from Fig. 1 are relabeled $F1$, $OB1$, and so forth. Catalyst $C0$ catalyzes the production of $OB0$ (which contains a subsequence identical to C from Fig. 1), which in turn catalyzes the production of $OB1$. The concentration of upstream catalyst $C0$ is constant, so initially $[OB0]$ increases linearly with time, which causes $[OB1]$ to increase quadratically with time (Fig. 3B). Eventually, the substrates and fuels are depleted, and the reaction halts, giving rise to an overall sigmoidal shape to the fluorescence traces (Fig. 3B). The model previously used can be extended to predict the behavior of this feedforward circuit data (SOM text S8).

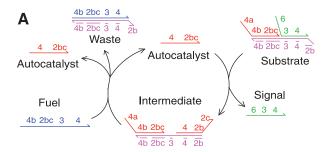This cascaded system can be used as an amplifier to detect small quantities of $C0$.

Repeated fluorescence experiments show that we are able to distinguish reliably between 1 pM (0.0001×) catalyst $C0$ and 0× catalyst within 12 hours (Fig. 3B, inset). This corresponds to a roughly 900-fold amplification of the input signal. (1 pM of catalyst triggered ≈ 900 pM of reporter above the baseline set by the 0× reaction.) For comparison, 1 pM corresponds to about one molecule per eukaryotic cell volume. Repeated measurements of independent samples show less than 3% variability across all timepoints (SOM text S9).
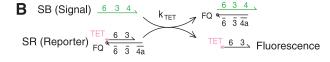
Feedback is another important feature of both biological regulatory networks and artificial control circuits. Exponential growth kinetics can be achieved by redesigning the reaction presented in Fig. 1 such that output OB contains catalyst C as a subsequence (Fig. 4A). The reaction is then autocatalytic. Figure 4C shows the time course of this reaction for a wide range of catalyst concentrations. In a process dominated by initial exponential growth ($c \approx c_0 e^{\lambda t}$), the time to reach a threshold degree of completion depends logarithmically on the initial concentration c_0 (where c is the concentration of the exponentially growing species, λ is the characteristic time constant, and t is time). Thus, a linear trend in a log-linear plot of initial concentration to time to half completion ($t_{1/2}$) is indicative of exponential growth. [Such plots are used as calibration standards for quantitation
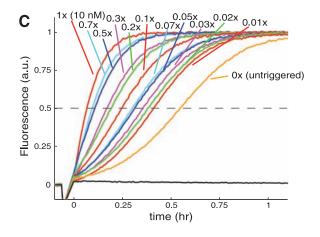
methods such as real-time polymerase chain reaction (PCR) (27).] Fig. 4D shows that our autocatalytic system has this characteristic behavior, implying that exponential growth kinetics have indeed been achieved and that the reaction is not substantially affected by product inhibition. Further confirmation comes from the quality of fit to the data of a model based on rate constants derived for the catalyst system of Fig. 1 (SOM text S8).

We also demonstrate feedback in a two-layer circuit by redesigning $OB1$ so that it can, in turn, catalyze the $F0 + S0$ reaction (SOM text S11). Feedback in this cross-catalytic system causes the concentrations of both $OB0$ and $OB1$ to grow exponentially at early times.

Largely because of their relevance to the origin of life and to the RNA world (1), autocatalytic and cross-catalytic self-replication reactions have been proposed and demonstrated previously (28). However, such systems typically suffer from product inhibition and thus exhibit parabolic, rather than exponential, growth kinetics. Recent exceptions include cross-catalytic deoxyribozymogens (13) and catalyzed self-assembly (29) based on the hybridization chain reaction (14); our autocatalyst system is faster than either of these. Reducing the spontaneous activity of the circuit (for example, by improved purification of the substrate complex) is an important goal for increasing the sensitivity to
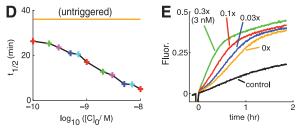

Fig. 4. The autocatalyst system. (**A**) Proposed reaction pathway. See table S2 for sequences of new domains. (**B**) Reporter complex *SR*, used for monitoring autocatalytic and cross-catalytic reaction networks. TET denotes the tetrachlorofluorescein fluorophore. FQ denotes the Iowa Black Fluorescent Quencher. (**C**) Kinetics of autocatalysis. Indicated amounts of autocatalyst were added at $t \approx 0$. At 30 min, 1% (100 pM) was amplified 25-fold over the untriggered reaction. Reporter *SR* was present at 20 nM = 2×. Control sample (black) contained no fuel *F*. (**D**) Semi-log plot of $t_{1/2}$ (in minutes) as a function of logarithm of molar trigger concentration. The orange line shows $t_{1/2}$ of the untriggered reaction. (**E**) Performance in the simultaneous presence of total RNA and unfractionated cell lysate. Total RNA present in solution was 10× (by mass) that of the sum of all relevant catalyst DNA. Active cell lysate, as would be used in an in vitro translation system, was added to be 1.1% by volume of total reaction (17 μL in 1500 μL). The control reaction did not contain any substrate *S*. Experiments involving total RNA but not cell lysates did not show the observed drift.

the point that our autocatalyst could be used as an enzyme-free constant-temperature alternative to PCR for detecting known sequences.

For many applications in biotechnology, nucleic acid devices must remain functional in the presence of naturally occurring macromolecules. We therefore tested the autocatalyst system in the presence of an excess of mouse liver total RNA with rabbit reticulocyte lysate (Fig. 4E). Reactions proceeded to apparent completion with no more than a twofold slowdown, and the presence of a 3% trigger can still be detected.

The ability to construct larger circuits will enable the wide range of chemical circuit functions needed for sophisticated applications. Our entropy-driven catalytic reaction networks are suited for scaling up to larger circuits. The modular molecular design makes synthesis of more complex components and networks with arbitrary topology straightforward. To demonstrate this, we constructed an entropy-driven catalytic analog AND gate in which both of two catalysts are required to release output (SOM text S12 and fig. S11). For scaling up to large circuits, independent catalyst systems must have negligible crosstalk. The success of quantitative models that assume no crosstalk, as presented above, is encouraging; further evidence comes from a test of two independent catalyst systems operating in the same solution (fig. S12). Finally, catalytic systems have the potential to avoid the slowdown that plagued previous attempts to construct large nucleic acid circuits (*17*).

Future nucleic acid control circuits must be interfaced to molecular sensors and actuators. This may be achieved directly when the inputs and outputs are themselves nucleic acids, such as for the detection, analysis, and response to complex nucleic acid samples (*9, 30*) or for the control of nucleic acid nanomachines (*2, 31*). Nucleic acid circuits can also respond to and control more general chemical events: In principle, the release of an oligonucleotide could regulate covalent chemistry by controlling (deoxy)ribozyme activity (*9*) or reactant proximity (*32*). Additionally, signals carried by small organics and other non–nucleic acid molecules can be read by nucleic acid systems with the use of aptamer domains (*33, 34*) and other binding interactions that can regulate toehold accessibility (*35, 36*). Thus, nucleic acids could provide a general-purpose system for the synthesis of embedded control circuitry within aqueous chemical systems.

References and Notes

1. R. F. Gesteland, T. R. Cech, J. F. Atkins, Eds. *The RNA World: The Nature of Modern RNA Suggests a Prebiotic RNA World* (Cold Spring Harbor Laboratory Press, Cold Spring Harbor, NY, ed. 3, 2006).
2. N. C. Seeman, *Trends Biochem. Sci.* **30**, 119 (2005).
3. J. Bath, A. J. Turberfield, *Nat. Nanotechnol.* **2**, 275 (2007).
4. G. F. Joyce, *Annu. Rev. Biochem.* **73**, 791 (2004).
5. A. J. Turberfield et al., *Phys. Rev. Lett.* **90**, 118102 (2003).
6. J. S. Bois et al., *Nucleic Acids Res.* **33**, 4090 (2005).
7. G. Seelig, B. Yurke, E. Winfree, *J. Am. Chem. Soc.* **128**, 12211 (2006).
8. S. J. Green, D. Lubrich, A. J. Turberfield, *Biophys. J.* **91**, 2966 (2006).
9. M. N. Stojanovic, T. E. Mitchell, D. Stefanovic, *J. Am. Chem. Soc.* **124**, 3555 (2002).
10. J. Macdonald et al., *Nano Lett.* **6**, 2598 (2006).
11. H. Lederman, J. Macdonald, D. Stefanovic, M. N. Stojanovic, *Biochemistry* **45**, 1194 (2006).
12. M. Hagiya, S. Yaegashi, K. Takahashi, in *Nanotechnology: Science and Computation*, J. Chen, N. Jonoska, G. Rozenberg, Eds. (Springer, New York, 2006), pp. 293–308.
13. M. Levy, A. D. Ellington, *Proc. Natl. Acad. Sci. U.S.A.* **100**, 6416 (2003).
14. R. M. Dirks, N. A. Pierce, *Proc. Natl. Acad. Sci. U.S.A.* **101**, 15275 (2004).
15. M. N. Stojanovic et al., *J. Am. Chem. Soc.* **127**, 6914 (2005).
16. R. Penchovsky, R. R. Breaker, *Nat. Biotechnol.* **23**, 1424 (2005).
17. G. Seelig, D. Soloveichik, D. Y. Zhang, E. Winfree, *Science* **314**, 1585 (2006).
18. In the system presented in Fig. 1, there is some sequence redundancy in the domain sequences chosen (for example, 2b and 5 are identical). This is because all four systems presented in this paper were designed together, with the goal of minimizing the number of differences between systems. In the design of a catalytic reaction in isolation, there are no sequence constraints; we demonstrate a system with completely independent catalyst and output in SOM text S10; it has very similar kinetics to that of the reaction shown in Fig. 1.
19. M. Zuker, *Nucleic Acids Res.* **31**, 3406 (2003).
20. J. Sager, D. Stefanovic, in *DNA Computing: 11th International Workshop on DNA Computing*, A. Carbone, N. A. Pierce, Eds. (Springer, Berlin, 2006), pp. 275–290.
21. K. U. Mir, in *DNA-Based Computers II: DIMACS Workshop*, L. F. Landweber, E. B. Baum, Eds. (American Mathematical Society, Providence, RI, 1999), pp. 243–246.
22. B. Yurke, A. P. Mills, *Genet. Program. Evolvable Mach.* **4**, 111 (2003).
23. I. G. Panyutin, P. Hsieh, *J. Mol. Biol.* **230**, 413 (1993).
24. Materials and methods (SOM text S2) are available as supporting material on *Science* Online.
25. S. A. Marras, F. R. Kramer, S. Tyagi, *Nucleic Acids Res.* **30**, e122 (2002).
26. C. Green, C. Tibbetts, *Nucleic Acids Res.* **9**, 1905 (1981).
27. R. Higuchi, G. Fockler, G. Dollinger, R. Watson, *Nat. Biotechnol.* **11**, 1026 (1993).
28. N. Paul, G. F. Joyce, *Curr. Opin. Chem. Biol.* **8**, 634 (2004).
29. P. Yin, H. M. T. Choi, C. R. Calvert, N. Pierce, *Nature*, in press.
30. Y. Benenson, B. Gil, U. Ben-Dor, R. Adar, E. Shapiro, *Nature* **429**, 423 (2004).
31. R. Pei et al., *J. Am. Chem. Soc.* **128**, 12693 (2006).
32. X. Li, D. R. Liu, *Angew. Chem. Int. Ed.* **43**, 4848 (2004).
33. A. D. Ellington, J. Szostak, *Nature* **346**, 818 (1990).
34. J. Tang, R. R. Breaker, *Chem. Biol.* **4**, 453 (1997).
35. S. Müller, D. Strohbach, J. Wolf, *Proc. IEEE Nanobiotechnol.* **153**, 31 (2006).
36. F. J. Isaacs, D. J. Dwyer, J. J. Collins, *Nat. Biotechnol.* **24**, 545 (2006).
37. We thank X. R. Bao, G. Seelig, D. Soloveichik, P. Rothemund, and L. Adleman for insightful discussions. There is a patent pending on this work. D.Y.Z. and A.J.T. were supported by UK research councils (Engineering and Physical Sciences Research Council, Biotechnology and Biological Sciences Research Council, Medical Research Council, and the Ministry of Defence) though the Bionanotechnology Interdisciplinary Research Collaboration. D.Y.Z. and E.W. were supported by a Caltech Grubstake Grant and NSF grants 0506468, 0622254, and 0533064. D.Y.Z. is supported by the Fannie and John Hertz Foundation.

Radar Sounding of the Medusae Fossae Formation Mars: Equatorial Ice or Dry, Low-Density Deposits?

Thomas R. Watters,[1]* Bruce Campbell,[1] Lynn Carter,[1] Carl J. Leuschen,[2] Jeffrey J. Plaut,[3] Giovanni Picardi,[4] Roberto Orosei,[4] Ali Safaeinili,[3] Stephen M. Clifford,[5] William M. Farrell,[6] Anton B. Ivanov,[3] Roger J. Phillips,[7] Ellen R. Stofan[8]

The equatorial Medusae Fossae Formation (MFF) is enigmatic and perhaps among the youngest geologic deposits on Mars. They are thought to be composed of volcanic ash, eolian sediments, or an ice-rich material analogous to polar layered deposits. The Mars Advanced Radar for Subsurface and Ionospheric Sounding (MARSIS) instrument aboard the Mars Express Spacecraft has detected nadir echoes offset in time-delay from the surface return in orbits over MFF material. These echoes are interpreted to be from the subsurface interface between the MFF material and the underlying terrain. The delay time between the MFF surface and subsurface echoes is consistent with massive deposits emplaced on generally planar lowlands materials with a real dielectric constant of ~2.9 ± 0.4. The real dielectric constant and the estimated dielectric losses are consistent with a substantial component of water ice. However, an anomalously low-density, ice-poor material cannot be ruled out. If ice-rich, the MFF must have a higher percentage of dust and sand than polar layered deposits. The volume of water in an ice-rich MFF deposit would be comparable to that of the south polar layered deposits.

Units of the Medusae Fossae Formation (MFF) occur discontinuously at equatorial latitudes along the boundary of the hemispheric dichotomy from Amazonis to Elysium Planitiae (~130°E to 240°E) (*1, 2*). The

MFF may be among the youngest surficial deposits on Mars, unconformably overlying ancient Noachian heavily cratered highlands and young Amazonian lowlands (*1–8*). However, pedestal craters on the outer edge of the MFF